JOURNAL OF SOLID STATE CHEMISTRY **141,** 466–474 (1998)
ARTICLE NO. SC987998

High-Temperature Neutron Diffraction Study of $Y_4Al_2O_9$

Hisanori Yamane[1] and Masahiko Shimada

Institute for Advanced Materials Processing, Tohoku University, 2-1-1 Katahira, Aoba-ku, Sendai 980-8577, Japan

and

Brett A. Hunter

Australian Nuclear Science and Technology Organisation, P.M.B., Menai, New South Wales 2234, Australia

Received March 30, 1998; in revised form August 7, 1998; accepted August 12, 1998

The anisotropic thermal expansion and anisotropy of lattice volume change in $Y_4Al_2O_9$ at 1370°C were confirmed by high-temperature neutron diffraction of the sintered polycrystalline sample. The cell volume of the high-temperature phase is approximately 0.4% smaller than that of the low-temperature phase. The crystal structure of the high-temperature phase was determined by Rietveld analysis. It crystallizes in a monoclinic cell, $a = 7.4804(4)$ Å, $b = 10.5461(5)$ Å, $c = 11.2057(7)$ Å, and $\beta = 108.927(4)^\circ$ at 1518°C, $Z = 4$ with space group $P2_1/c$, which is identical to the space group of the low-temperature phase. The phase transition was concluded to be diffusionless by comparison of the crystal structures of the high- and low-temperature phases. At the transition, the atoms in the unit cell move cooperatively on the slip planes of oxygen atoms parallel to the (010) plane along the *a* axis.

INTRODUCTION

Zirconia (ZrO_2) and zirconia-dispersed ceramics exhibit high strength because the volume increase of the martensitic transition from the high-temperature tetragonal phase, stabilized in the ceramics, to the low-temperature monoclinic phase acts to close the crack and reduce the driving force for crack extension (1). The phase transition of ZrO_2 is reversible. A large hysteresis between the starting temperatures of the forward (cooling) and reverse (heating) transitions is seen around 1000°C. Such thermal hysteresis is one of the characteristics of the martensitic transformation. In the martensitic phase transition, the amount of a transformed phase is independent of time, but a function of temperature only (athermal). The transformation is displacive and diffusionless and takes place by a shear mechanism. The thermal hysteresis width was considerably influenced by the stress applied to the crystal and by chemical composition.

Recently, high-temperature phase transformations in other ceramic materials have been investigated for possible alternative transformation tougheners to zirconia (2). Studies by differential scanning calorimetry and dilatometry revealed reversible phase transitions in $Y_4Al_2O_9$ and other rare-earth aluminates $RE_4Al_2O_9$ or gallates $RE_4Ga_2O_9$ (RE = rare-earth elements) above 1000°C (3–9). The phase transitions have thermal hysteresis and a volume decrease of about 0.5% on heating from the low-temperature phase to the high-temperature phase. The hysteresis widths, of between 15 and 200°C, were found to be affected by the grain size and rare-earth elements (6, 7). The phase transition temperature, defined by the average of transition temperatures on heating and cooling, was 1377°C for $Y_4Al_2O_9$ (5) and varied in the $RE_4Al_2O_9$ and $RE_4Ga_2O_9$ systems, depending on the ionic radii of RE^{3+} and Al^{3+} or Ga^{3+} ions (8). Athermal, nonthermal-activated character and a stabilization effect were observed at the phase transition of $Y_4Al_2O_9$ (7). These results have suggested that the phase transition of $Y_4Al_2O_9$ is martensitic.

Brandle and Steinfink determined the crystal structure of $Eu_4Al_2O_9$ by single-crystal X-ray diffraction and found it to form in a monoclinic cell, space group $P2_1/c$ (10). This structure is isostructural with cuspidine, $Ca_4Si_2O_7F_2$ (11). The atomic positions of $Y_4Al_2O_9$ were refined with the structure model of $Eu_4Al_2O_9$ by Lehmann *et al.* using high-resolution X-ray synchrotron powder data (12) and by Christensen and Hazell using X-ray and neutron single-crystal data (13). In the crystal structure of $Y_4Al_2O_9$ the Al atoms are coordinated to four oxygen atoms. Isolated, double-tetrahedral groups (Al_2O_7) are formed by AlO_4 tetrahedra sharing a single apical oxygen atom. The Y atoms are coordinated to either six or seven oxygen atoms.

[1] To whom correspondence should be addressed. E-mail: yamane@iamp.tohoku.ac.jp.

0022-4596/98 $25.00

A high-temperature study observed discontinuities and anisotropic changes of the lattice parameters of $Y_4Al_2O_9$ at 1400°C using high-temperature X-ray powder diffraction (XRD) (5). The diffraction peaks in the patterns of the high-temperature phase taken at 1450 and 1500°C were also indexed with monoclinic cells with space group $P2_1/c$ (5, 6, 14). Shull *et al.* (6) tried to explain the pattern of 1500°C based on the pseudo-orthorhombic and pseudo-cubic unit cells proposed by Reed and Chase (15) and Brandle and Steinfink (10). However, they could not index the reflections in the pattern completely using either of these proposed unit cells.

The unit cell volume, from high-temperature XRD, of the $Y_4Al_2O_9$ high-temperature phase at 1400°C obtained by cooling from 1450°C was 0.5% smaller than that of the low-temperature phase at the same temperature of 1400°C obtained by heating from room temperature (5). This volume change was in accordance with the results of dilatometry. The relative intensities of the main reflections in the XRD pattern of the high-temperature phase were not significantly different from those of the low-temperature phase (14). This suggested that the crystal structures of the two phases did not differ significantly from each other. The oxygen positions in the high-temperature

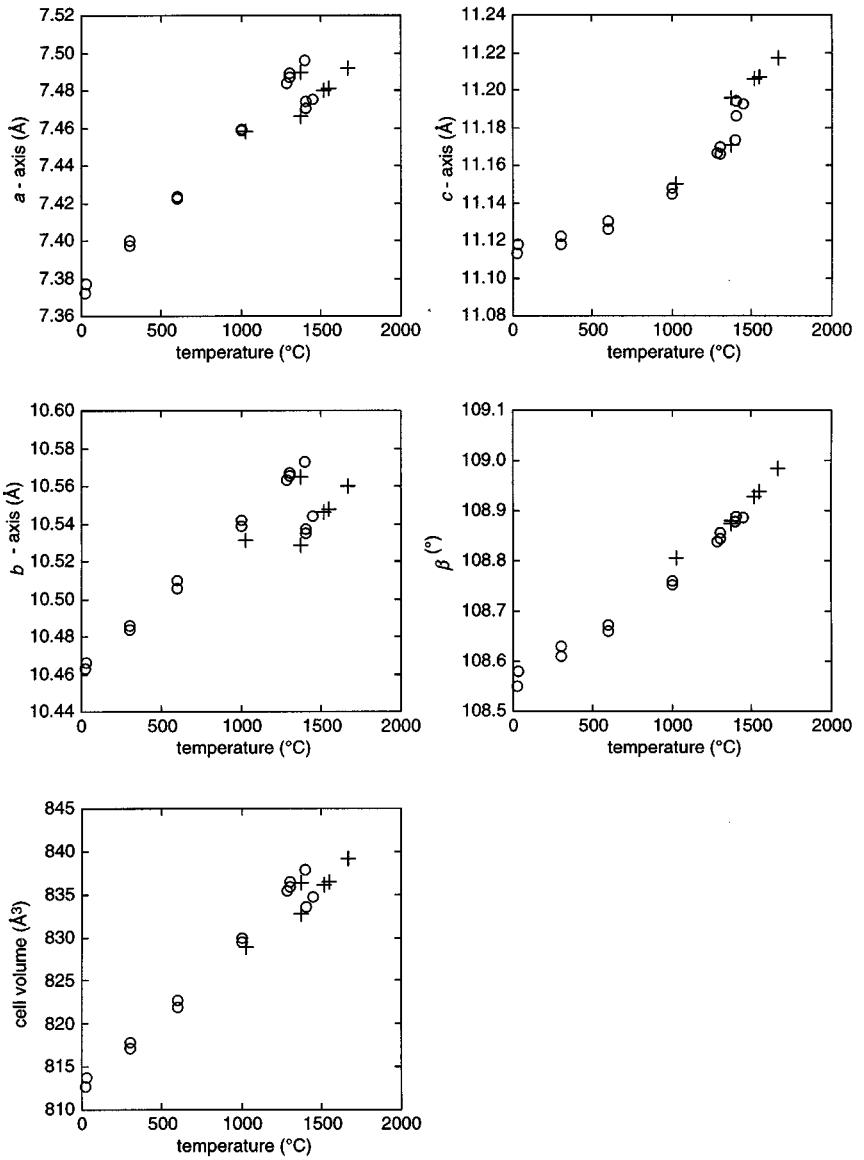

FIG. 1. Temperature-dependent variation of the monoclinic lattice parameters and cell volume for $Y_4Al_2O_9$: (○) X-ray powder diffraction (4); (+) neutron diffraction.

phase could not be determined by Rietveld analysis of the XRD pattern (14), although the positions of the Y atoms were refined with the room temperature structural model.

As mentioned above, the results of the previous studies have suggested that the phase transition of $Y_4Al_2O_9$ is diffusionless and martensitic. However, it necessary to determine the crystal structure of the high-temperature phase to clarify the mechanism of the phase transition of $Y_4Al_2O_9$. In the present paper, we will establish the crystallographic relationship between the structures of the high- and low-temperature phases of $Y_4Al_2O_9$ as determined by high-temperature neutron powder diffraction and discuss the high-temperature phase transformation.

EXPERIMENTAL

Y_2O_3 powder (99.99% purity, Mitsubishi Kasei Corp.) and Al_2O_3 powder (99.9% purity, Sumitomo Chemical Corp., Ltd.) were weighed with a molar ratio $Y:Al = 2:1$. The powders were mixed by ball-milling with an appropriate amount of ethanol. The powder slurry was then dried and pressed into pellets. Polycrystalline ceramic pellets of $Y_4Al_2O_9$ were prepared from these pellets by reaction sintering at 1600°C for 5 h on a Pt 70%–Rh 30% plate. The sintered pellets were 12 mm in diameter and approximately 7 mm thick. The bulk density was 97% of the theoretical density of $Y_4Al_2O_9$. The grain size of $Y_4Al_2O_9$ was less than 20 μm.

Neutron diffraction data for the $Y_4Al_2O_9$ ceramics were collected on the medium–high-resolution neutron powder diffractometer (MHRPD) at the HIFAR reactor operated by the Australian Nuclear Science and Technology Organisation, using neutrons of wavelength 1.664 Å in the range $10° < 2\theta < 128°$ with a step width of 0.1°. The $Y_4Al_2O_9$ ceramic pellets were piled up to form a rod about 80 mm in height and placed on the Pt–Rh plate. This was then placed in a high-temperature furnace on the diffractometer. The heater elements of the furnace were molybdenum silicide (Kanthal 1800). The temperature stability was approximately ±3°C. The incident and diffracted neutron beams passed through an alumina insulator and an aluminum window 50 mm in width. A 2θ range from 63.5° to 69.0° was excluded during refinement because of absorption by the heater elements. Rapid scan data were taken at various temperatures from 1025 to 1665°C to check the phase transition. The data for structure refinement were collected at 1025 and 1518°C with sufficient scan rates to obtain maximum peak intensities of 3000 counts in each detector. The data from each detector were summed to form a single pattern.

The atomic positions of $Y_4Al_2O_9$ reported by Christensen and Hazell (13) were used for the starting model of the low-temperature phase. The model of the high-temperature phase was found by trial and error. Preliminary Rietveld refinements were undertaken with a PC version of the computer program LHPM (16). The final structure refinements were carried out by using RIETAN (17). The coherent neutron scattering lengths and cross sections of atoms were used as given in the RIETAN software. An absorption correction was performed in the RIETAN program using analytical approximation of absorption factors for the cylindrical sample. The background was refined with eight parameters simultaneously with other profile parameters. A pseudo-Voigt function was used to fit the lineshape of the neutron diffraction patterns. The width of the Gaussian component was varied as $\sigma^2 = U\tan^2\theta + V\tan\theta + W$,

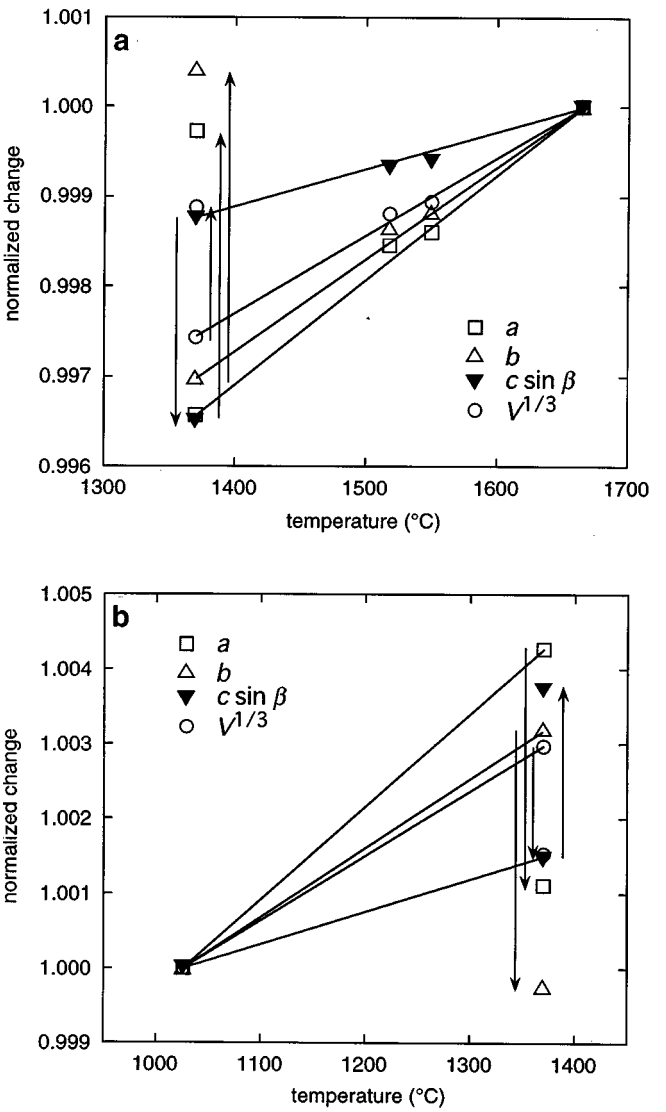

FIG. 2. Temperature dependence of lattice parameters a, b, $c \sin\beta$, and (cell volume, V)$^{1/3}$ normalized with the values at 1665 (a) and 1025°C (b).

where U, V, and W are refinable parameters. Since the Scherrer broadening parameter, X, in the width of the Lorentzian component, $X \sec\theta + Y \tan\theta$, tended to be very small minus the value during the refinement, X was fixed to be zero, and only the microstrain broadening parameter, Y, was refined. An asymmetry parameter, P, was fixed at the instrumental value because of a large correlation with the lattice parameters. In the final structural refinement, 77 parameters were varied, including one zero-point shift, 8 background, 4 peak shape, 45 positional, and 14 isotropic thermal parameters. The thermal parameters of aluminum atoms, Al1 and Al2, were constrained to be equal. Interatomic distances and bond angles, together with estimated standard deviations, were computed using the program ORFFE (18). Structure graphics were drawn using ATOMS (19).

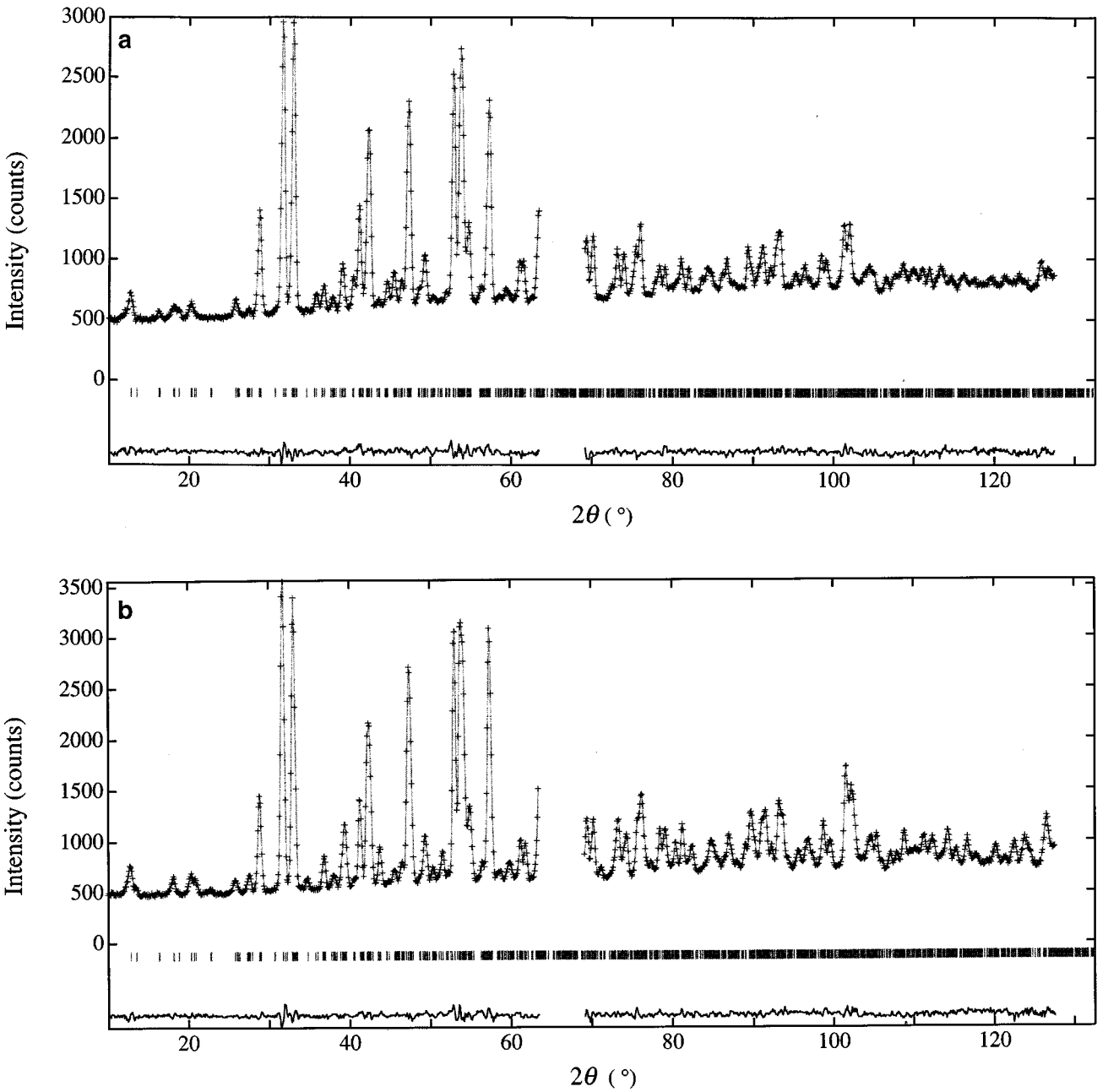

FIG. 3. Observed, calculated, and difference neutron diffraction profiles for $Y_4Al_2O_9$ at 1518 (a) and 1025°C (b). The observed data are indicated by crosses and the profiles calculated by the Rietveld refinement and the differences between the observed and calculated patterns are shown by solid lines. The short vertical lines below the profiles mark the position of all possible Bragg reflections.

RESULTS AND DISCUSSION

All peaks in the high-temperature neutron diffraction patterns of $Y_4Al_2O_9$ were indexed in monoclinic cells with space group $P2_1/c$. As shown in Fig. 1, the lattice parameters of $Y_4Al_2O_9$ at various temperatures obtained by neutron diffraction were comparable with the values reported by X-ray powder diffraction (5). The unit cell volume of the low-temperature phase measured on heating to 1370°C was approximately 0.4% larger than the high-temperature phase obtained on cooling to the same temperature. This was consistent with the volume change measured by high-temperature dilatometry. The *a*- and *b*-axis lengths contracted and the *c*-axis length expanded at the phase transition from the low-temperature phase to the high-temperature phase with almost the same β angle.

The anisotropic changes were also seen for thermal expansion coefficients in the plots of normalized lattice parameters (Fig. 2). The rates of thermal expansions perpendicular to the *a*–*b* planes ($c \sin \beta$) are smaller than those along other directions for both the high- and low-temperature phases. The $c \sin \beta$ direction, having small thermal coefficients, shows a reverse change against the other directions at the phase transition. The anisotropic transformation seems to compensate the change of anisotropic thermal expansion. We speculate that the sheer stress derived from the anisotropic thermal expansion in $Y_4Al_2O_9$ ceramics influences the starting and finishing temperatures of the martensitic phase transformation.

Figure 3 shows the profile fit and difference patterns of the Rietveld analysis for the neutron diffraction patterns of the high- and low-temperature phases at 1518 and 1025°C,

TABLE 1
Structure and Thermal-Displacement Parameters of $Y_4Al_2O_9$

		x	*y*	*z*	*B* (Å^2)
Y1	1025°C	0.5244(11)	0.1080(8)	0.7870(8)	2.5(2)
	1518°C	0.275(2)	0.1034(10)	0.7950(10)	3.1(2)
Y2	1025°C	0.0237(10)	0.0955(6)	0.8050(6)	1.25(14)
	1518°C	0.781(2)	0.0966(10)	0.8095(10)	3.6(3)
Y3	1025°C	0.3379(11)	0.1215(8)	0.4337(7)	2.0(2)
	1518°C	0.084(2)	0.1260(10)	0.4256(10)	2.9(2)
Y4	1025°C	0.8363(11)	0.1237(8)	0.4169(7)	1.9(2)
	1518°C	0.5914(14)	0.1183(10)	0.4224(10)	2.4(2)
Al1	1025°C	0.217(2)	0.181(2)	0.1320(14)	1.7(2)
	1518°C	0.950(4)	0.178(2)	0.126(2)	2.7(2)
Al2	1025°C	0.639(2)	0.1800(14)	0.1098(14)	1.7
	1518°C	0.397(3)	0.186(2)	0.106(2)	2.7
O1	1025°C	0.790(2)	0.2314(11)	0.7489(10)	2.7(2)
	1518°C	0.524(2)	0.2210(13)	0.7507(12)	3.4(3)
O2	1025°C	0.2373(13)	0.2367(9)	0.7690(8)	1.4(2)
	1518°C	0.986(2)	0.2393(13)	0.7607(12)	3.2(3)
O3	1025°C	0.214(2)	0.0235(11)	0.1607(11)	2.6(2)
	1518°C	0.940(3)	0.022(2)	0.1396(13)	5.4(5)
O4	1025°C	0.0737(13)	0.2342(11)	0.9834(9)	3.1(2)
	1518°C	0.816(2)	0.237(2)	0.9800(12)	4.4(3)
O5	1025°C	0.431(2)	0.2366(8)	0.1137(10)	2.9(2)
	1518°C	0.178(4)	0.2145(13)	0.118(2)	7.0(3)
O6	1025°C	0.6303(13)	0.2304(9)	0.9570(8)	2.0(2)
	1518°C	0.380(2)	0.2427(12)	0.9634(12)	2.3(2)
O7	1025°C	0.698(2)	0.0281(13)	0.1528(12)	3.4(2)
	1518°C	0.474(2)	0.0311(14)	0.1719(13)	2.9(6)
O8	1025°C	0.083(2)	−0.0041(11)	0.3939(13)	2.8(2)
	1518°C	10.828(2)	−0.0020(11)	0.391(2)	2.8(3)
O9	1025°C	0.563(2)	0.0057(9)	0.3878(11)	1.5(2)
	1518°C	0.317(3)	−0.0092(12)	0.391(2)	3.5(3)

TABLE 2
Interatomic Distances (Å) in $Y_4Al_2O_9$

1025°C		1518°C	
Y1–O9	2.199(13)	Y1–O8	2.24(2)
–O6	2.217(12)	–O7	2.29(2)
–O3	2.307(14)	–O6	2.32(2)
–O7	2.44(2)	–O3	2.37(2)
–O5	2.456(13)	–O1	2.42(2)
–O2	2.487(13)	–O2	2.52(2)
–O1	2.517(14)	–O5	2.69(2)
Y2–O1	2.185(14)	Y2–O1	2.25(2)
–O3	2.303(14)	–O9	2.31(2)
–O2	2.306(12)	–O3	2.34(2)
–O8	2.311(14)	–O2	2.34(2)
–O7	2.37(2)	–O4	2.37(2)
–O4	2.398(11)	–O7	2.39(2)
Y3–O8	2.24(2)	Y3–O2	2.26(2)
–O9	2.265(14)	–O8	2.27(2)
–O2	2.298(12)	–O8	2.34(2)
–O9	2.313(13)	–O9	2.38(2)
–O5	2.417(13)	–O6	2.53(2)
–O6	2.625(11)	–O5	2.64(2)
–O4	2.684(13)	–O4	2.69(2)
Y4–O4	2.254(14)	Y4–O4	2.20(2)
–O6	2.316(14)	–O9	2.29(2)
–O9	2.318(14)	–O8	2.29(2)
–O1	2.353(13)	–O6	2.31(2)
–O8	2.36(2)	–O9	2.38(2)
–O8	2.363(14)	–O1	2.49(2)
–O7	2.97(2)	–O7	2.81(2)
Al1–O3	1.69(2)	Al1–O3	1.65(3)
–O2	1.72(2)	–O2	1.69(2)
–O4	1.75(2)	–O4	1.73(3)
–O5	1.77(2)	–O5	1.78(4)
Al2–O5	1.68(2)	Al2–O6	1.67(2)
–O7	1.69(2)	–O5	1.70(4)
–O6	1.76(2)	–O7	1.81(3)
–O1	1.85(2)	–O1	1.87(2)

TABLE 3
Bond Angles (Å) in $Y_4Al_2O_9$

1025°C		1518°C	
O4–Al1–O5	94.8(9)	O2–Al1–O5	93.2(14)
O2–Al1–O5	96.4(9)	O4–Al1–O5	98 (2)
O3–Al1–O2	109.2(11)	O3–Al1–O5	107 (2)
O3–Al1–O5	114.2(11)	O3–Al1–O4	115 (2)
O3–Al1–O4	116.8(10)	O3–Al1–O2	115 (2)
O2–Al1–O4	122.3(11)	O2–Al1–O4	122 (2)
O5–Al2–O1	96.7(8)	O5–Al2–O1	94.3(12)
O5–Al2–O6	99.8(9)	O7–Al2–O1	96.6(11)
O7–Al2–O1	102.0(10)	O6–Al2–O5	103.6(14)
O6–Al2–O1	118.8(9)	O5–Al2–O7	108 (2)
O5–Al2–O7	119.0(10)	O6–Al2–O1	120.1(14)
O7–Al2–O6	119.1(10)	O6–Al2–O7	128.5(13)
Al1–O5–Al2	139.7(9)	Al1–O5–Al2	157.3(13)

respectively. The refined lattice parameters were $a = 7.4804(4)$ Å, $b = 10.5461(5)$ Å, $c = 11.2057(7)$ Å, and $\beta = 108.927(4)^\circ$ at 1518°C and $a = 7.4579(3)$ Å, $b = 10.5310(4)$ Å, $c = 11.1498(5)$ Å, and $\beta = 108.806(3)^\circ$ at 1025°C. The diffraction pattern taken at 1025°C was fitted well with the structural model of $Y_4Al_2O_9$ at room temperature. The final R factors as proposed by Wiles and Young (20) were $R_{wp} = 2.41$, $R_p = 1.93$, $R_B = 1.66$, and $R_F = 1.13\%$ for the refinement of the low-temperature phase. When we adopted the structural model of the low-temperature phase for the refinement of the high-temperature phase, R_{wp} was around 5%, and the peaks having large intensities were fitted well. However, the small peaks could not be fitted adequately, which suggests an atomic rearrangement of the unit cell.

The hint we used to solve the structure of the high-temperature phase was the very small intensity of the 100 reflection in the diffraction pattern of the high-temperature phase. We tried to find a configuration of the Al_2O_7 groups, which decreased the 100 intensity and kept the arrangement of Y and oxygen atoms almost the same as that of the low-temperature phase. The structural model of the best fit was obtained by shifting atomic positions by $a/4$ along the a axis. The final R factors were $R_{wp} = 2.33$, $R_p = 1.82$, $R_B = 2.98$, and $R_F = 1.86\%$. The final positional and thermal parameters for the high- and low-temperature phases are given in Table 1, and selected interatomic distances and bond angles are listed in Tables 2 and 3, respectively.

Figure 4 shows the perspective view of atomic arrangements for the high- and low-temperature phases along the b axis with y from -0.03 to $+0.27$, illustrating the oxygen coordination around the Y and Al atoms. From this view, the atomic arrangements of the high- and low-temperature phases are almost unchanged. The numbers of O atoms

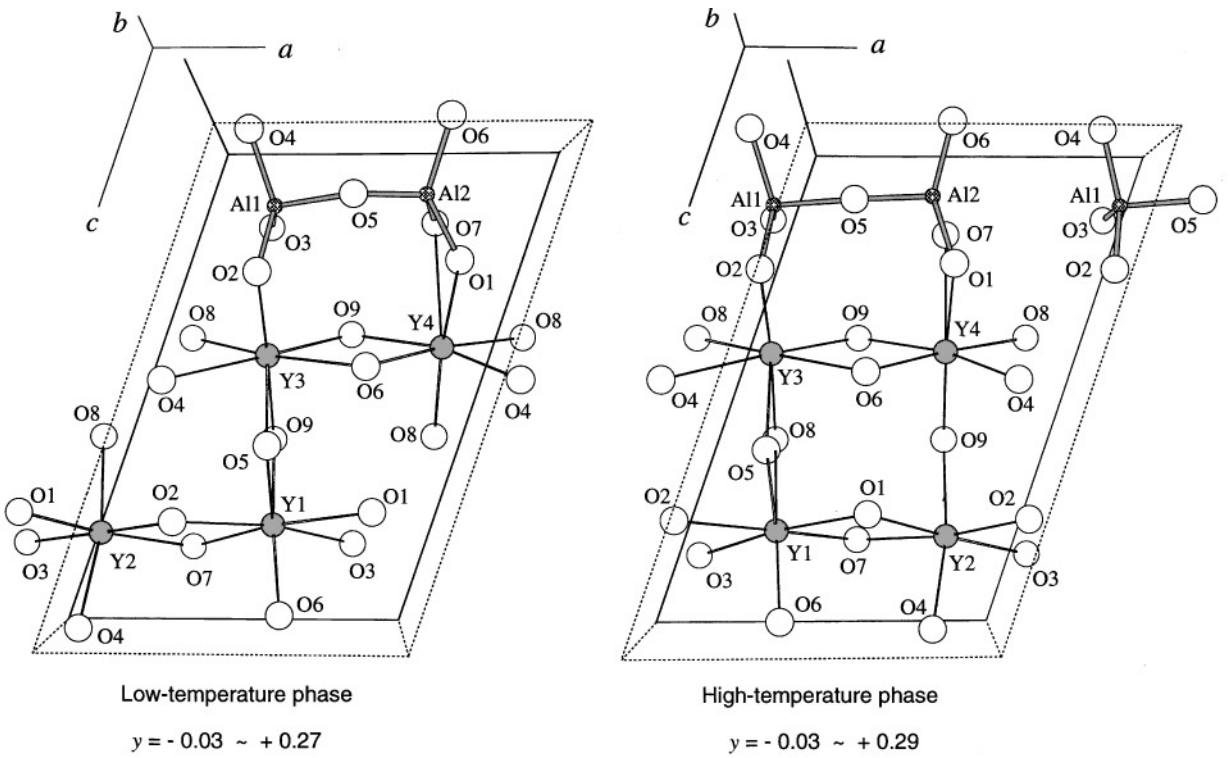

FIG. 4. Perspective views of $Y_4Al_2O_9$ structures for the high- and low-temperature phases along the b axis showing oxygen atom coordination around Al and Y atoms within 3.0-Å interatomic distances.

surrounding the Y atoms within the interatomic distances of 0–3.0 Å are the same in both phases: six for the Y2 atoms and seven for the Y1, Y3 and Y4 atoms (Table 3 and Fig. 4). The Al1–O5–Al2 bond angle in the Al_2O_7 aluminate anions of the high-temperature phase is larger than that in the low-temperature phase. The larger angle is favorable if we consider electrostatic repulsion of nonshared oxygen atoms in the Al_2O_7 anions.

The projections of the crystal structures are drawn with AlO_4 tetrahedra along the *b*, *c*, and *a* axes in Figs. 5a, 5b, and 5c, respectively. The crystal structure of $Y_4Al_2O_9$ can be described as a layered structure stacking along the *b* axis, as seen in Figs. 5b and 5c. Y and Al atoms were situated between the two kinds of oxygen layers. Oxygen atoms of the layers around $y = 1/4$ and $3/4$ (O1, O2, O4, O5) are coordinated to Al and Y atoms. In the other layers around $y = 0$ and $1/2$, O3 and O7 are apical oxygen atoms of the Al_2O_7 groups, and the O8 and O9 atoms are coordinated to the Y atoms only. From these views, the arrangements of Al_2O_7 with the *c*-glide relation are almost same in the unit

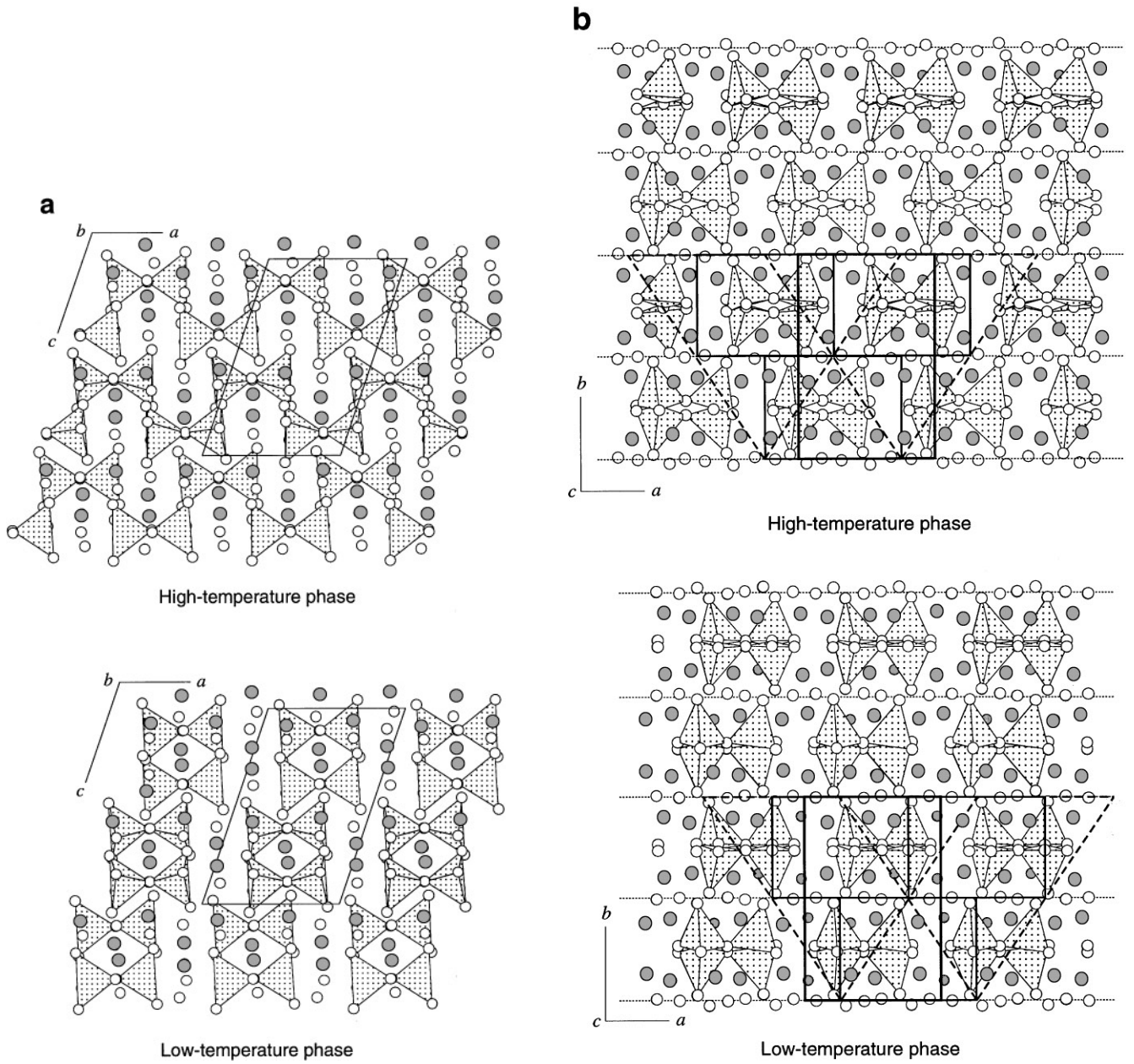

FIG. 5. Crystal structures of $Y_4Al_2O_9$ high- and low-temperature phases projected on the *a*–*c* plane (a), the *a*–*b* plane (b), and the *b*–*c* plane (c) with AlO_4 tetrahedra. O and Y atoms are shown with open and filled circles, respectively.

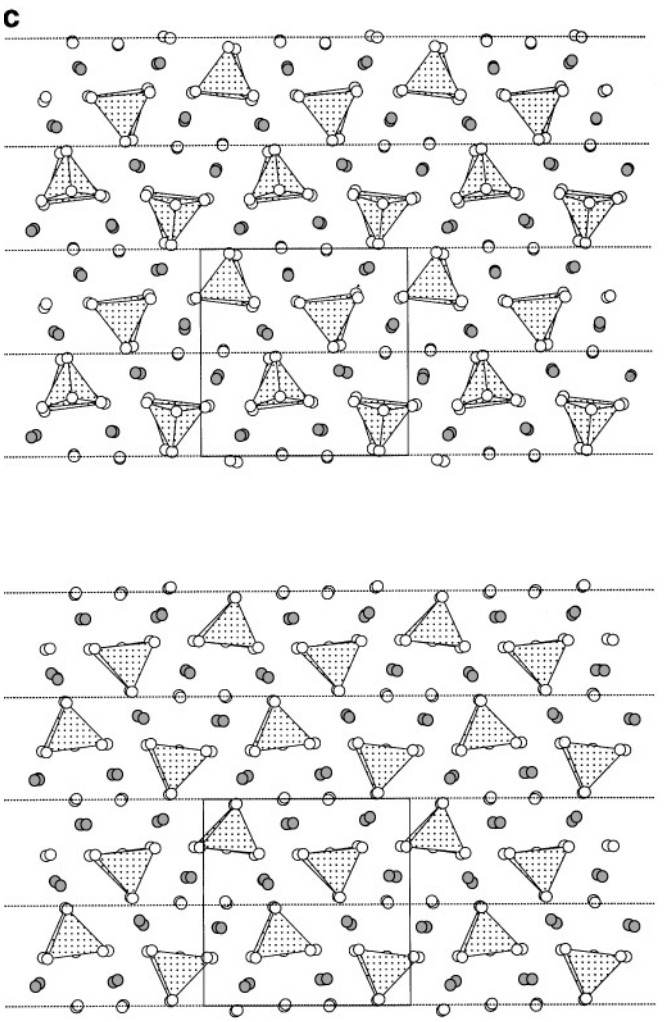

FIGURE 5—*Continued*

from $y = 0$ to $1/2$ for both phases, but the unit shifts on the a–c plane and along the a axis by $a/4$ (Fig. 5b). The difference of the unit stacking is also explained in terms of the $a/4$ displacement of a 2_1 screw axis along the a axis.

It is unlikely that the structure is changed at the phase transition by detachment of the bridging atoms O5 from the Al atoms and by subsequent migration to the vacant sites between the Al1 and Al2 atoms. From the comparison between the structures of the high- and low-temperature phases, we conclude that the atoms move cooperatively, and each unit slips on the a–c plane around $y = 0$ and $1/2$ and along the a axis by $a/4$ (about 1.9 Å) at the phase transition of $Y_4Al_2O_9$. Figure 6 shows the projections of the structures on the a–b plane, illustrating a movement of the $b/2$ unit layers along the a axis by $a/4$ at the transformation from the low-temperature phase to the high-temperature phase. This phase transition is diffusionless and related to a martensitic transformation as suggested by the previous studies (4–7). In the martensitic transition, the lattice distortion and the transformation shear are usually reduced by slip or twinning associated with the transition. For the transformation of $Y_4Al_2O_9$ accompanying the large deformation of the original cell, the slip planes are inherent on the (010) planes at every $b/2$ period.

Twinning of $Y_4Al_2O_9$ was reported in the previous studies on the preparation of single crystals and on the structures of sintered polycrystalline samples (6, 7, 21–23). A twin plane of (100) was determined by X-ray Weissenberg photo-

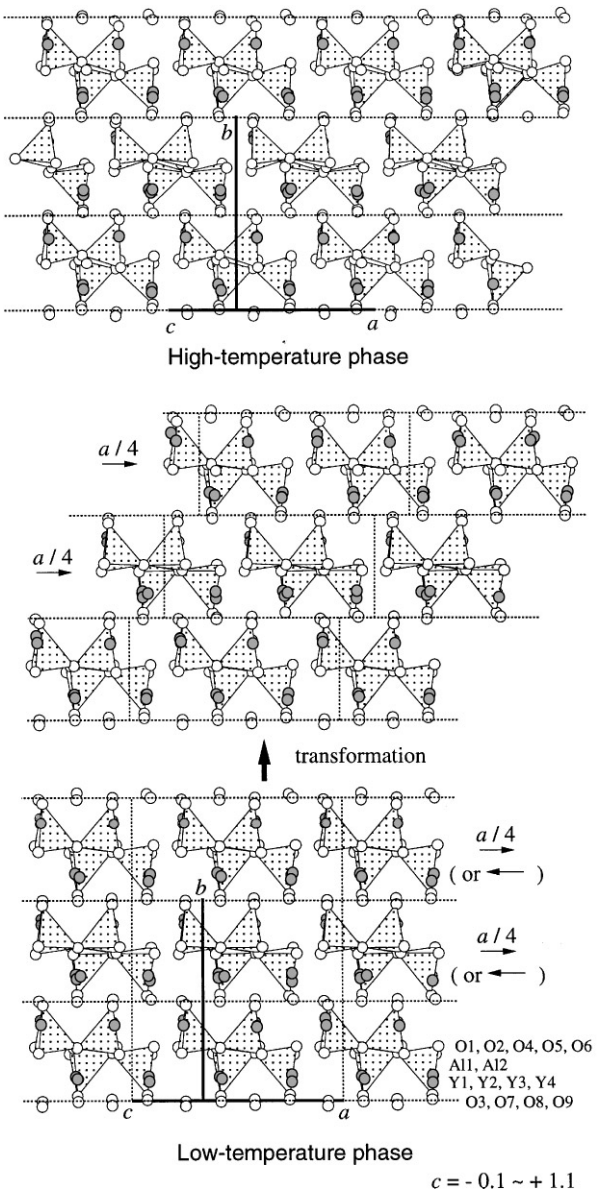

FIG. 6. Crystal structures of $Y_4Al_2O_9$ high- and low-temperature phases projected on the a–b plane with AlO_4 tetrahedra, illustrating a shift of the $b/2$ unit layers along the a axis by $a/4$ (about 1.9 Å) at the phase transition from the low-temperature to high-temperature phases. O and Y atoms are shown with open and filled circles, respectively.

graphs (21). No change was observed for this twining from room temperature to 1600°C, which is more than 200°C above the phase transition temperature (5, 21). The twin plane could not be introduced by the displacement of atoms at the transition. The mechanism of the (100) twin formation might be a mechanical twinning caused by the sheer stress at the phase transformation on cooling. Another possibility is by an order–disorder phase transformation at a higher temperature between 1665°C and the melting point (about 2000°C (9, 24)). Recently, a disorder arrangement of Si_2O_7 groups has been shown in the structure analysis of an isostructural compound $Ca_2Y_2Si_2O_9$ (25).

ACKNOWLEDGMENTS

This work was partly supported by the Ministry of Education, Science, Sports and Culture, Japan, by the Nippon Sheet Glass Foundation for Materials Science and Engineering, and by NEDO under the Synergy Ceramics Project of the Industrial Science and Technology Frontier Program promoted by AIST, MITI, Japan. M.S. is a member of the Joint Research Consortium of Synergy Ceramics.

REFERENCES

1. D. J. Green, R. H. J. Hannink, and M. V. Swain, "Transformation Toughening of Ceramics." CRC Press, Boca Raton, FL, 1989.
2. W. M. Kriven, *J. Am. Ceram. Soc.* **71,** 1021 (1988).
3. P. D. Jero and W. M. Kriven, *J. Am. Ceram. Soc.* **71,** C454 (1988).
4. M. Omori, Z. Chen, T. Koide, and T. Hirai, *in* "Proceedings of the 1st International Symposium on the Science of Engineering Ceramics" (S. Kimura and K. Niihara, Eds.), p. 515. The Ceramic Society of Japan, Tokyo, 1991.
5. H. Yamane, M. Omori, A. Okubo, and T. Hirai, *J. Am. Ceram. Soc.* **76,** 2382 (1993).
6. J. L. Shull, W. M. Kriven, W. D. Porter, and C. R. Hubbard, *in* "Solid → Solid Phase Transformations" (W. C. Johnson, J. M. Howe, D. E. Lauglin, and W. A. Soffa, Eds.), p. 95. The Minerals, Metals & Materials Society, Warrendale, Pennsylvania, 1994.
7. H. Yamane, K. Ogawara, M. Omori, and T. Hirai, *J. Am. Ceram. Soc.* **78,** 1230 (1995).
8. H. Yamane, K. Ogawara, M. Omori, and T. Hirai, *J. Am. Ceram. Soc.* **78,** 2385 (1995).
9. M. Grevais and A. Douy, *Mater. Sci. Eng.* **B38,** 118 (1996).
10. C. D. Brandle and H. Steinfink, *Inorg. Chem.* **8,** 1320 (1969).
11. S. Saburi, A. Kawahara, and C. Henmi, *Mineral. J.* **8,** 286 (1977).
12. M. S. Lehmann, A. N. Christensen, H. Fjellvåg, R. Feidenhans'l, and M. Nielsen, *J. Appl. Crystallogr.* **20,** 123 (1987).
13. A. N. Christensen and R. G. Hazell, *Acta Chem. Scand.* **45,** 226 (1991).
14. H. Yamane, M. Omori, and T. Hirai, *J. Mater. Sci. Lett.* **14,** 470 (1995).
15. J. W. Reed and A. B. Chase, *Acta Crystallogr.* **15,** 812 (1962).
16. R. J. Hill and C. J. Howard, Australian Atomic Energy Commission Report No. M112, AAEC (now ANSTO), Lucas Heights Research Laboratories, New South Wales, Australia, 1986.
17. F. Izumi, *in* "The Rietveld Method" (R. A. Young, Ed.), p. 236. Oxford Univ. Press, London, 1993.
18. W. R. Busing, K. O. Martin, and H. A. Levy, Report ORNL-TM-306, Oak Ridge National Laboratory, Oak Ridge, TN, 1964.
19. E. Dowty, "ATOMS: A Computer Program for Displaying Atomic Structures," Shape Software, Kingsport, TN, 1991.
20. R. A. Young, *in* "The Rietveld Method" (R. A. Young, Ed.), p. 1. Oxford Univ. Press, London, 1993.
21. N. A. Toropov, I. A. Bondar, F. Ya. Galadhov, Kh. S. Nikogosyan, and N. V. Vinogradova, *Izv. Akad. Nauk SSR, Ser. Khim.* **7,** 1158 (1964).
22. M. Omori, A. Sakuma, and T. Hirai, *in* "Ceramics Today—Tomorrow's Ceramics" (P. Vincenzini, Ed.), p. 1327. Elsevier Science, Amsterdam/New York, 1991.
23. H. Yamane, M. Omori, and T. Hirai, *J. Mater. Sci. Lett.* **14,** 561 (1995).
24. T.-I. Mah and M. D. Petry, *J. Am. Ceram. Soc.* **75,** 2006 (1992).
25. H. Yamane, T. Nagasawa, Y. Murakami, T. Kamata, D. Shindo, and M. Shimada, *Mater. Res. Bull.* **33,** 845 (1998).